

SUPERRESOLUTION AND EDGE-PRESERVING RECONSTRUCTION OF COMPLEX-VALUED SYNTHETIC APERTURE RADAR IMAGES

Müjdat Çetin and W. Clem Karl

Multi-Dimensional Signal Processing Laboratory, Dept. of ECE
Boston University, 8 Saint Mary's Street, Boston, MA 02215, USA

ABSTRACT

We propose a regularization-based method for the complex-valued synthetic aperture radar (SAR) image formation problem. The method can produce images with higher resolution than that supported by the measured data, as well as images with reduced variability of reflectivity magnitudes within homogeneous regions and preserved region boundaries. This is achieved by the inclusion of prior information in the regularized data inversion process through non-quadratic potential functions. For this task, we demonstrate the use of a variety of potential functions in our framework. The technique effectively deals with the random-phase nature of the underlying SAR reflectivities. For an efficient numerical solution, we extend half-quadratic regularization methods to this complex-valued problem. We demonstrate the performance of the method on real SAR data.

1. INTRODUCTION

Synthetic aperture radar (SAR) is a sensor which synthesizes high-resolution terrain maps using data gathered from multiple observation angles. Data are collected by a radar traversing a flight path and pointing in the direction of a ground patch to be imaged. The all-weather nature, potentially high resolution, and large area coverage rates of the phenomenology have led to its increased use in surveillance, as well as growing interest in automated processing techniques, wherein features extracted from the formed imagery are used for automatic object detection and recognition.

The conventional technique for the formation of this imagery is the polar format algorithm [1]. This approach, while straightforward, has certain shortcomings. First, the resolution of the formed images is limited by the SAR system bandwidth. This complicates point scatterer localization for automated recognition tasks. In addition, the images

suffer from speckle, which complicates region segmentation for shape-based recognition.

To alleviate these problems, we develop a new technique for SAR image formation, which can produce both super-resolution images and reduced-speckle, edge-preserved images within the same framework. The method is based on the incorporation of prior information regarding the features of interest together with an explicit model relating the SAR observations to the underlying scene in a regularized image reconstruction framework. Our method is an extension of real-valued image reconstruction methods to the complex-valued, random-phase SAR problem. Prior information regarding the underlying scene or features of interest are captured through a set of non-quadratic constraints, which leads to potentially costly optimization problems. We develop an efficient iterative method for solving the resulting problems by extending half-quadratic optimization methods. We demonstrate the performance of the method on real SAR scenes.

2. IMAGE RECONSTRUCTION METHOD

2.1. Overview

We start from the following assumed discrete model for the SAR observation process:

$$y = Tf + w \quad (1)$$

where y represents projectional SAR observations, f is the unknown sampled reflectivity image, w is additive measurement noise, all column stacked as vectors, and T is a complex-valued tomographic SAR observation matrix [2, 3]. In this framework, the objective of SAR image reconstruction is to obtain an estimate of f based on the data y . The conventional SAR polar format image formation algorithm can roughly be interpreted in this framework as the application of the adjoint to the data: $\hat{f} = T^H y$.

In contrast, we formulate the SAR image reconstruction problem as an optimization problem of the following form:

$$\hat{f} = \arg \min_f [\|y - Tf\|_2^2 + \Psi(f)] \quad (2)$$

This work was supported by the Air Force Office of Scientific Research under Grant F49620-96-1-0028, the National Institutes of Health under Grant NINDS 1 R01 NS34189, and the Army Research Office under Grant ARO DAAG55-97-1-0013.

where $\Psi(f)$ is a function from \mathbb{C}^N to $\mathbb{R}^+ \cup \{0\}$. The first term in the right-hand-side expression in (2) is a data fidelity term. The second term is a constraint reflecting the prior information we would like to impose. The reconstruction naturally depends on the kind of constraint used, hence the choice of $\Psi(f)$ is critical.

2.2. Choice of $\Psi(f)$

A simple and common choice in many conventional regularization schemes is to set $\Psi(f)$ to be a quadratic function of f (or its derivatives), which leads to Tikhonov regularization. In a variety of imaging problems, it has been observed that this choice may suppress useful features in the image, such as edges. Furthermore, since the image reconstruction in this case essentially amounts to linear processing of the data, resolution improvements cannot be achieved.

Recently, alternative, non-quadratic constraints have been proposed for increasing the resolution in spectral analysis [4, 5], as well as for edge-preserving smoothing in real-valued image restoration and reconstruction problems [6–10]. In our work, we extend the use of such feature-preserving prior models to the problem of complex-valued SAR imaging.

We aim to use such prior models in a single framework for two types of objectives: increasing the resolution, and decreasing the variability within homogeneous regions without suppressing region boundaries. Consequently, we will have a separate term for each objective in $\Psi(f)$. In particular, we choose $\Psi(f)$ as follows:

$$\Psi(f) = \lambda_1^2 \sum_i \psi(|(f)_i|) + \lambda_2^2 \sum_i \psi((D|f|)_i). \quad (3)$$

Here, λ_1 and λ_2 are scalar parameters, D is a discrete 2-D derivative operator and $(\cdot)_i$ denotes the i th element of a vector. The role of the first term in (3) is to put an energy-type constraint on the solution, and this term should be chosen in such a way to suppress artifacts and increase the resolvability of scatterers. The second term is a piecewise smoothness penalty which should be chosen in such a way that it provides the required smoothing while preserving the edges and hence the shapes of the objects.¹ The relative magnitudes of λ_1 and λ_2 reflect the emphasis on superresolution imaging and edge-preserving smoothing respectively.

Smoothness penalties used in real-valued imaging problems are usually based on Df . For the SAR imaging problem however, we need to impose smoothness on the *magnitudes* of the complex-valued, random-phase field f , therefore our constraint is in terms of $D|f|$. Note that the non-linearity introduced by this SAR-based constraint can create

¹Our method does not require the potential functions ψ used for the two terms in (3) to be identical, however we use identical potential functions for simplicity here.

$\psi_1(x)$	$(x^2 + \beta)^{p/2}$
$\psi_2(x)$	$\frac{(x^2 + \beta)^{p/2}}{1 + (x^2 + \beta)^{p/2}}$
$\psi_3(x)$	$\log(1 + (x^2 + \beta)^{p/2})$

Table 1. Families of potential functions used. p is a parameter determining the shape of the functions. β is a small smoothing constant.

a more challenging optimization problem than that arising in real-valued image reconstruction problems based on Df .

Now, let us discuss the choice of the potential function ψ . In [11], we have used potential functions based on ℓ_1 -norms, here we will consider more general priors. The three particular classes of feature-preserving functions ψ we will use in this paper are shown in Table 1.² For all of these functions, β is a small smoothing parameter, hence $(x^2 + \beta)^{p/2} \approx x^p$. Using such a smooth approximation to x^p prevents numerical complications which may arise in differentiating x^p around the origin for $p \leq 1$.

Note that the use of ψ_1 in (3) leads to constraints in terms of approximate ℓ_p -norms [6], where we will consider values of p smaller than 1. The potential function ψ_2 is based on previous work in [7]. Special cases of ψ_2 for $p = 1$ and $p = 2$ yield the potential functions used in [8] and [9] respectively. Finally, ψ_3 is a generalized version of the potential function proposed in [10]. Note that these potential functions can more generally be expressed in terms of x/Δ , where Δ is a scaling parameter. We will use a fixed Δ , and omit it in our analysis for notational simplicity.

2.3. Numerical Solution

The optimization problem in (2) with the particular choices of ψ (hence Ψ) we have made, does not have a closed-form solution. For its numerical solution, we will use a quasi-Newton method with a particular Hessian approximation. Our method can also be shown to be an extension of the half-quadratic regularization scheme of [8]. To this end, we first take the gradient of the expression in (2) with respect to the real and imaginary parts of f . Then, using a compact notation with complex-valued matrices, we write the resulting optimality condition in terms of what resembles a linear function of f :

$$\tilde{H}(f)f = 2T^H y \quad (4)$$

where

$$\tilde{H}(f) \triangleq 2T^H T + \lambda_1^2 Q_k(|f|) + \lambda_2^2 \Phi^H(f) D^T Q_k(D|f|) D \Phi(f) \quad (5)$$

²One might subtract an appropriate constant from each potential function to set $\psi_k(0) = 0$ ($k = 1, 2, 3$), however we have chosen not to do so in Table 1, to keep the notation simpler.

$q_1(x)$	$\frac{p}{(x^2+\beta)^{1-p/2}}$
$q_2(x)$	$\frac{p}{(x^2+\beta)^{1-p/2} [(x^2+\beta)^{p/2+1}]^2}$
$q_3(x)$	$\frac{p}{(x^2+\beta)^{1-p/2} [(x^2+\beta)^{p/2+1}]}$

Table 2. The weighting functions associated with the potential functions.

$$Q_k(z) \triangleq \text{diag} \{q_k(z_i)\}$$

$$\Phi(f) \triangleq \text{diag} \{\exp(-j\phi[(f)_i])\}$$

Here $\phi[(f)_i]$ denotes the phase of the complex number $(f)_i$, and $\text{diag}\{\cdot\}$ is a diagonal matrix whose i th diagonal element is given by the expression inside the brackets. The weighting functions $q_k(\cdot)$ ($k = 1, 2, 3$) depend on the potential functions ψ_k , and are shown in Table 2.

To compute the solution, we will use a quasi-Newton-type algorithm, where $\tilde{H}(f)$ at each step of the algorithm will serve as the Hessian approximation for the next iteration. This leads to the following iteration for $\hat{f}^{(n+1)}$:

$$\tilde{H}(\hat{f}^{(n)}) \hat{f}^{(n+1)} = (1 - \gamma) \tilde{H}(\hat{f}^{(n)}) \hat{f}^{(n)} + \gamma 2T^H y \quad (6)$$

where γ is the step-size. We terminate the iteration whenever the ℓ_2 -norm of the difference between consecutive iterates, relative to the norm of the iterate itself, is smaller than a threshold.

3. EXPERIMENTAL RESULTS

To demonstrate the performance of our image reconstruction method, we use images from the MIT Lincoln Laboratory Advanced Detection Technology Sensor (ADTS) data set [12]. For all the results presented here, we have chosen the values of λ_1 and λ_2 based on subjective qualitative assessment of the formed imagery. We use $\Delta = 1$ for all the examples.

First, we will consider edge-preserving image formation in our framework. For this task, the dominant prior information term in (3) should be the smoothness constraint (hence we need to set $\lambda_2 > \lambda_1$). Images of a military vehicle obtained by the use of various potential functions, as well as the conventional method are shown in Figure 1. The images produced by our scheme exhibit reduced speckle, and clear object and shadow boundaries which are important for automated decision making.

Next, we will demonstrate superresolution imaging. For this task, we set $\lambda_2 = 0$ in (3). Figure 2 shows images of the vehicle reconstructed from 0.6 m resolution data. Images formed by our approach exhibit improved resolution, reduced sidelobes and hence better dominant scatterer localization than the conventional image. Figure 3 contains

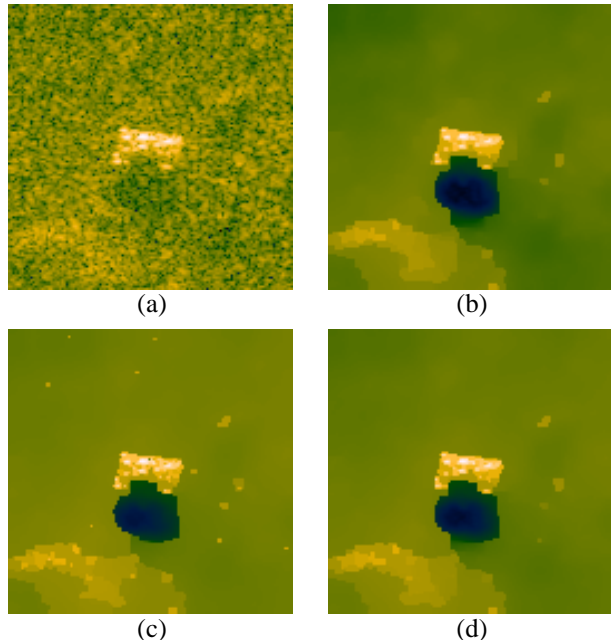


Fig. 1. Edge-preserving reconstructions with various potential functions. (a) Conventional image. (b) ψ_1 , $p = 0.8$. (c) ψ_2 , $p = 0.8$. (d) ψ_3 , $p = 0.8$.

similar results for an even more reduced resolution level of 1.2 m.

For a quantitative evaluation of this image formation technique (for a subset of the potential functions used here) in terms of feature-preserving accuracy, please see [13].

4. CONCLUSIONS

We have developed an enhanced regularized image formation method for the complex-valued SAR imaging problem, and demonstrated the use of three classes of feature-preserving potential functions in our framework. The method effectively deals with well-known difficulties in SAR such as resolution loss, sidelobes and speckle, and produces images which accentuate features important for automated interpretation of SAR imagery.

5. REFERENCES

- [1] J. Walker, "Range-Doppler imaging of rotating objects," *IEEE Trans. Aerosp. Electron. Syst.*, vol. AES-16, no. 1, pp. 23–52, 1980.
- [2] D. C. Munson Jr., J. D. O'Brien, and W. K. Jenkins, "A tomographic formulation of spotlight-mode synthetic aperture radar," *Proc. IEEE*, vol. 71, pp. 917–925, Aug. 1983.

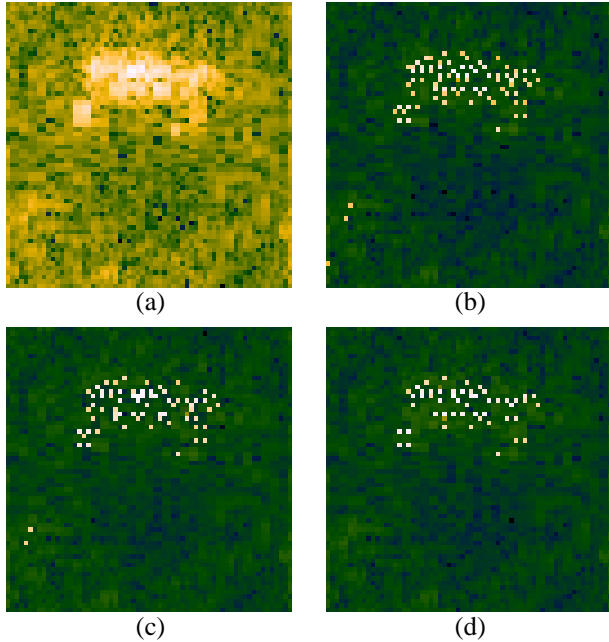


Fig. 2. Superresolution imaging from 0.6 m resolution data. (a) Conventional image. (b) $\psi_1, p = 0.8$ (c) $\psi_2, p = 0.8$. (d) $\psi_3, p = 0.8$.

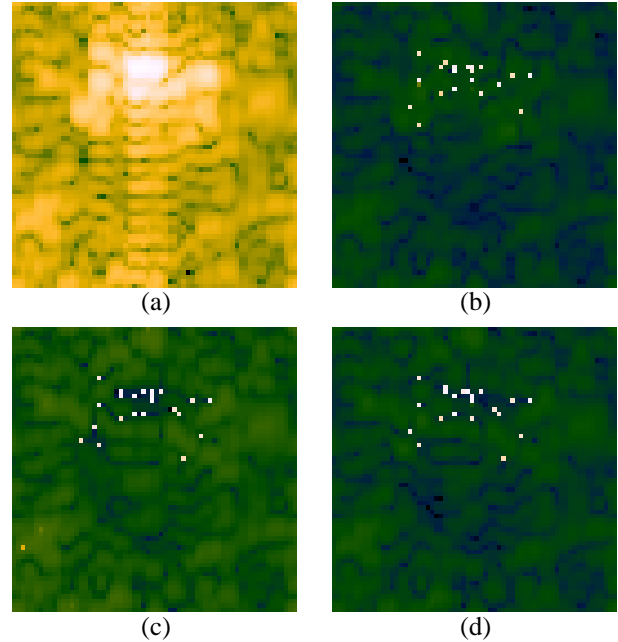


Fig. 3. Superresolution imaging from 1.2 m resolution data. (a) Conventional image. (b) $\psi_1, p = 0.8$ (c) $\psi_2, p = 1$. (d) $\psi_3, p = 0.8$.

- [3] M. Çetin and W. C. Karl, "A statistical tomographic approach to synthetic aperture radar image reconstruction," in *IEEE International Conference on Image Processing*, Santa Barbara, CA, Oct. 1997, vol. 1, pp. 845–848.
- [4] D. L. Donoho, I. M. Johnstone, J. C. Koch, and A. S. Stern, "Maximum entropy and the nearly black object," *J. R. Statist. Soc. B*, vol. 54, no. 1, pp. 41–81, 1992.
- [5] P. Ciuciu, J. Idier, and J. F. Giovannelli, "Markovian high resolution spectral analysis," in *IEEE International Conference on Acoustics, Speech and Signal Processing*, Phoenix, AZ, March 1999, vol. 3, pp. 1601–1604.
- [6] C. R. Vogel and M. E. Oman, "Fast, robust total variation-based reconstruction of noisy, blurred images," *IEEE Trans. Image Processing*, vol. 7, no. 6, pp. 813–824, June 1998.
- [7] S. Geman and D. E. McClure, "Statistical methods for tomographic image reconstruction," in *Proc. 46th Sess. Int. Stat. Inst. Bulletin ISI*, 1987, vol. 52.
- [8] D. Geman and G. Reynolds, "Constrained restoration and the recovery of discontinuities," *IEEE Trans. Pattern Anal. Machine Intell.*, vol. 14, no. 3, pp. 367–383, March 1992.
- [9] P. Charbonnier, L. Blanc-Féraud, G. Aubert, and M. Barlaud, "Deterministic edge-preserving regularization in computed imaging," *IEEE Trans. Image Processing*, vol. 6, no. 2, pp. 298–310, Feb. 1997.
- [10] T. Hebert and R. Leahy, "A generalized EM algorithm for 3-D Bayesian reconstruction from Poisson data using Gibbs priors," *IEEE Trans. Med. Imag.*, vol. 8, pp. 194–202, June 1989.
- [11] M. Çetin and W. C. Karl, "Enhanced, high resolution radar imaging based on robust regularization," in *IEEE International Conference on Acoustics, Speech, and Signal Processing*, İstanbul, Turkey, June 2000.
- [12] J. C. Henry, "The Lincoln Laboratory 35 GHz airborne polarimetric SAR imaging system," in *IEEE Nat. Telesyst. Conf.*, Atlanta, GA, March 1991, pp. 353–358.
- [13] M. Çetin, W. C. Karl, and D. A. Castañon, "Evaluation of a regularized SAR imaging technique based on recognition-oriented features," in *Algorithms for Synthetic Aperture Radar Imagery VII*, E. G. Zelnio, Ed., Orlando, FL, April 2000, vol. 4053 of *Proc. SPIE*.